JOURNAL OF Materials CHEMISTRY

Synthesis and crystal structure and optical properties of fluorenic-core oligomers

Silvia Destri,[a] Mariacecilia Pasini,[a] Chiara Botta,[a] William Porzio,*[a] Fabio Bertini[a] and Luciano Marchiò[b]

[a]*Istituto di Chimica delle Macromolecole del C.N.R., via E.Bassini 15, 20133 Milano, Italy. E-mail: rx@icm.mi.cnr.it*
[b]*Dipartimento di Chimica Generale ed Inorganica, Chimica Analitica, Chimica Fisica, Università di Parma, Parco Area delle Scienze, I-43100 Parma*

Received 5th October 2001, Accepted 24th January 2002
First published as an Advance Article on the web 4th March 2002

Fluorenic core oligomers, displaying interesting photoluminescence properties, have been synthesized by an organometallic route. The crystal and molecular structure of a fluorene derivative and three homologous oligomers have been studied. The spiro-derivative of dibromofluorene shows a very strong interaction between the H and Br atoms. The thienyl-terminated oligomer with a spiro-substituent adopts a particular herringbone arrangement with overlap of only the end-thienyl residues, conformationally disordered. The crystal of the all-phenyl derivative consists of the packing of discrete molecules cofacially arranged. The molecule with linear alkyl chains on the 9-position of the fluorene core and thienyl rings as end-groups exhibits polymorphism and its crystal structure, tetragonal, is very peculiar because of the loose packing allowing a good separation among adjacent thienyl rings.

The absorption and emission properties of this series were investigated and the electroluminescence of single-layer devices was characterized. The photoluminescence properties of the molecules are strongly dependent on their structural organization, displaying a red-shift of the emission from the amorphous phase, to the crystalline structure, to the aggregated form.

A comparison of the packing of these oligomers and oligothienylenes fully accounts for the optical properties of the reported molecules.

Introduction

The relevant optoelectronic properties of conjugated oligomers, either thienylene or phenylene based, used in the fabrication of devices, and their role as suitable model compounds to understand the properties of related polymers are well known and documented.[1–3] Specifically because of the remarkable dependence of these properties on supramolecular organization, the determination of both the molecular packing and conformations constitutes a crucial point in understanding the electronic properties,[4] hence improving the performance of devices developed.[2] In view of this, fluorene and polyfluorenes have been receiving great attention especially as active layers in light emitting diode (LED) prototypes[5,6] or back-light components in liquid crystal (LC) devices.[7]

A thorough knowledge of the relationship between the crystal packing and the resulting charge transport and optical properties addresses the strategy of increasing either the charge carrier mobility in field effect transistors (FET) and LED or photoluminescence (PL) quantum yield in the latter displays.[8]

The recent study of thiophene–fluorene oligomers and their polyesters[9] is directed towards this goal. To pursue this objective a very detailed characterization of intermolecular interactions is required. On the other hand the insertion of various substituents in the molecular main-frame strongly modifies both the solid state arrangement and the optical properties.

In fact copolymers of fluorene with a great number of comonomers ranging from benzene, stilbene to anthracene and spiro-bridge substituted fluorene have been prepared in order to avoid aggregate formation during the operation of LEDs[6] all emitting in blue region. Specifically, the introduction of a spiro-bridge to connect conjugated molecules can minimize the parallel aggregation and increase the PL intensity.[10]

With this in mind, here we report on the preparation of differently substituted oligomers, obtained by the addition of 2-thienyl, phenyl and *p*-cyanophenyl groups to a fluorene core, namely linear side chains (molecule **6** in Scheme 1) linked to fluorene as a protecting group or a spiro-cyclopentane residue at the same positions (molecules **7**, **8**, **9** respectively in Scheme 1). The aim of this work is to relate the structural features of different solid state organizations to the optical properties of the molecules as a function of their different chemical structure. In particular, we analyse the variations of the photoluminescence properties of the molecules going from the solution to different solid state arrangements.

Results and discussion

Synthesis

Organometallic coupling reactions have been employed to prepare 2,7-di(2-thienyl)-9,9-dihexylfluorene **6**, 2′,7′-di(2-thienyl)spiro[cyclopentane-1,9′-fluorene] **7**, 2′,7′-diphenylspiro-[cyclopentane-1,9′-fluorene] **8** and 2′,7′-bis(4-cyanophenyl)spiro-[cyclopentane-1,9′-fluorene] **9**, as described in Scheme 1. The acidic protons in the 9-position of fluorene were removed by lithiation followed by alkylation[11] with two equivalents of bromohexane to give **1**, while reaction with 1,4-dibromobutane afforded the cyclopentane derivative **3**. Bromination following the literature procedure[12] with bromine and $FeCl_3$ resulted in

 DOI: 10.1039/b109089p

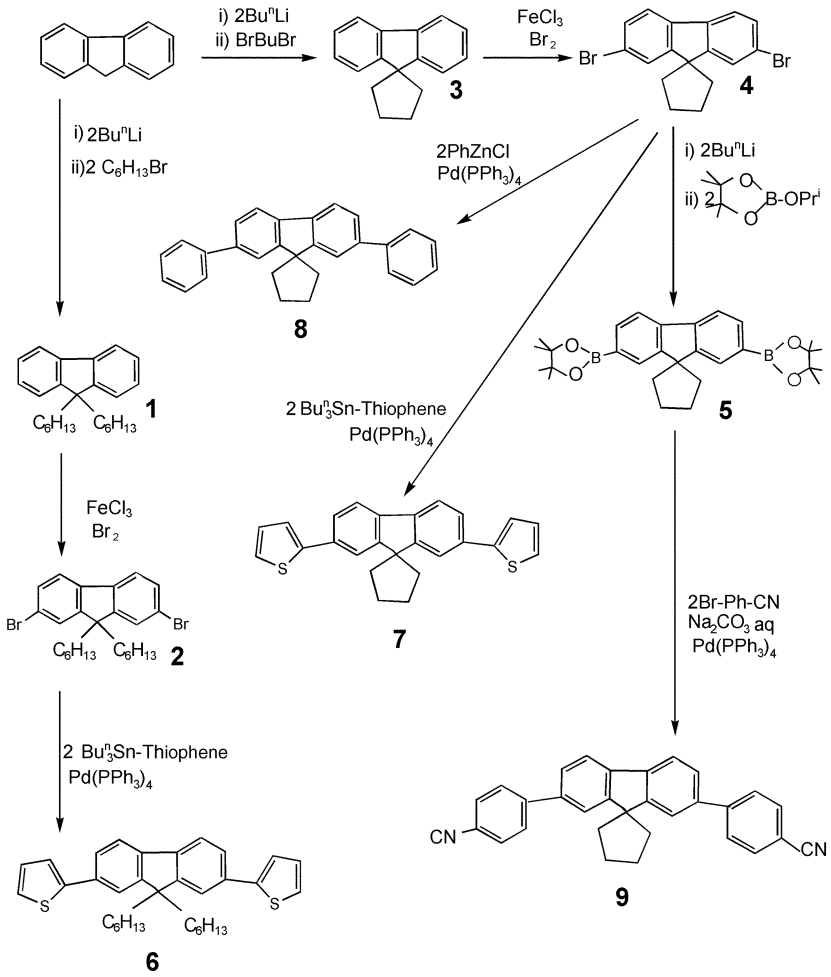

Scheme 1

the formation of the dibromides **2** and **4** in high yields. Both dibromides gave Stille[13] cross-coupling products with 2-(tributylstannyl)thiophene catalysed by $Pd(PPh_3)_4$ in refluxing toluene, affording 2,7-di(2-thienyl)-9,9-dihexylfluorene **6** and 2′,7′-di(2-thienyl)spiro[cyclopentane-1,9′-fluorene] **7** respectively. The spirofluorene derivative **4** is more reactive with respect to the corresponding compound **2**; in fact after 10 hours almost all of **4** had reacted while **2** needed a whole day to accomplish the reaction. The yields are comparable with that reported in the literature for the preparation of a similar compound *i.e.* 2,7-di(2-thienyl)-9,9-didecylfluorene with $Pd(PPh_3)_4$–$PdCl_2(PPh_3)$ 1 : 1 as catalysts.[14] As a side reaction, the self-coupling of the tin compound took place. The target compound **8** was synthesized by Pd catalysed coupling of 2′,7′-dibromospiro[cyclopentane-1,9′-fluorene] **4** with phenylzinc chloride. **4** could be transformed into bis(dioxaborolane) derivative **5** *via* lithiation in THF and quenching with 2-isopropoxy-4,4,5,5-tetramethyl-1,3,2-dioxaborolane. We slightly modified the literature procedure[15] in order to avoid both the alkylation of the fluorene core and the formation of the mono(dioxaborolane) derivative. To accomplish a suitable compromise an accurate check of temperature and time of both the two steps of the reaction had to be adopted.

The Suzuki reaction[16] of **5** with 4-bromobenzonitrile in toluene and aqueous Na_2CO_3 gave in high yield the target oligomer with two cyano groups **9**.

In the following the crystal and molecular structures of **4**, **6**, **7** and **8** are reported. The detailed study of the structure of **4** is justified by the presence of a fluorenic core; in contrast the structure of **8** could be solved only at an approximate level, due to the crystal quality (see Experimental section).

Structure of 4†

The bond distances and bond angles are as expected and supplied as supplementary material. The ORTEP drawing of **4** with labels is shown in Fig. 1.

The geometrical features of the present structure (bond distances, angles and torsions) are clearly comparable with those observed in 2,7-dibromo-9,9-dioctylfluorene.[17] In both cases the fluorene moiety is planar within 0.02 Å. The cyclopentane ring adopts an envelope conformation displaying an angle of 144° between the [C(14)–C(15)–C(16)–C(17)] and [C(9)–C(14)–C(17)] planes. Moreover the cyclopentane moiety and the fluorenyl residue are nearly orthogonal. However, a different packing arrangement is expected in view of the dioctyl *versus* cyclopentane substitutions.

Indeed the molecular packing, viewed along the *c* axis (see Fig. 2) consists of alternating sheets of molecules, forming angles close to 85° and linked together by the hydrogen–bromine interactions, as also observed in 1,2,3,4 tetrabromobenzene crystals.[18] In fact the H(16) and Br(2) normalized distance is of 2.91 Å is significantly shorter than any analogous distance in tetrabromobenzene polymorphs.[18] Other intermolecular contacts involving both Br–C and C–C atoms exceed the sum of commonly accepted van der Waals radii. Hence the key factor keeping the molecular sheets together is the formation of strong H···Br interactions (see Fig. 2).

†CCDC reference number 158135. See http://www.rsc.org/suppdata/jm/b1/b109089p/ for crystallographic files in .cif or other electronic format.

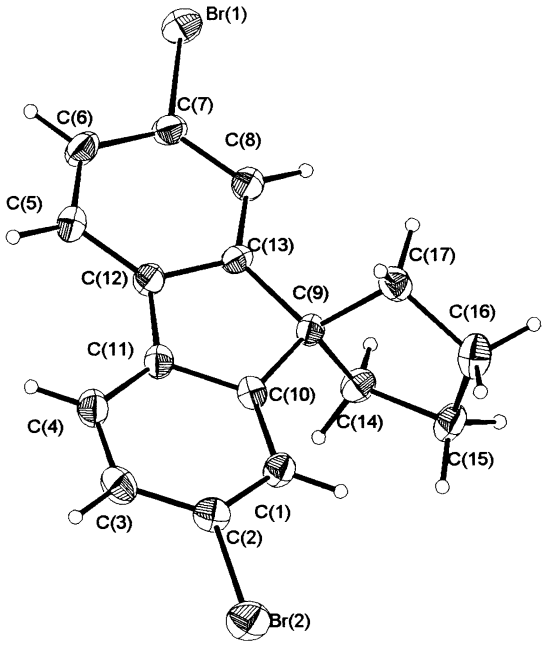

Fig. 1 ORTEP drawing of **4**, with numbering scheme, the ellipsoid probability is 30%.

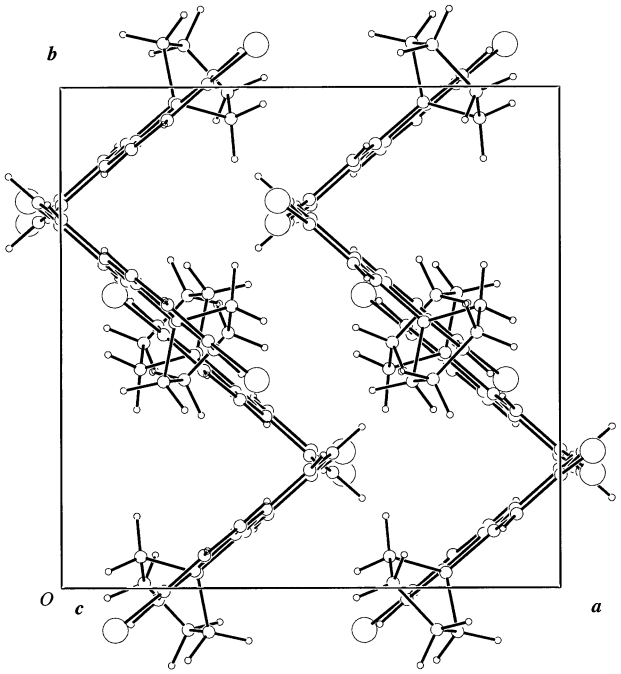

Fig. 2 Unit cell content of **4**, as viewed along the *c* axis.

Structure of 6‡

This molecule was studied by DSC, optical microscopy and XRD, and showed polymorphism.

In Fig. 3 DSC scans of **6** are reported. Two endothermic peaks are clearly observed in the first heating run with onsets at 72 °C and 113 °C. Corresponding enthalpies are ~3 mJ mol^{-1} and ~93 mJ mol^{-1}. In the second run (cooling rate −5 °C min^{-1}) no exothermic peak is detectable, indicating a slow crystallization rate; in fact the subsequent heating (rate 20 °C min^{-1}) shows a small endothermic peak above 115 °C. The optical microscopy observations are in agreement with the above results: indeed some brightness appears near 80 °C followed by complete clearing at 122 °C. Hence, the first peak is attributed to a conformation transition of the hexyl chain, as the enthalpy involved is comparable to that calculated for a *trans* to *gauche* transition in a hydrocarbon chain,[19] while the second peak is attributed to the melting point.

Temperature XRD analysis on **6** powders corroborates the suggestion of chain disordering, since above 80 °C the pattern is quite similar to that observed at room temperature, except for *a huge peak broadening*, while above 130 °C only a broad peak of the amorphous phase is detected.

From crystal structure analysis (see Table 1 for details) it is possible to perform line profile analyses of three intense low angle peaks, belonging to the [112], [121] and [202] directions respectively; then an attribution of this mesophase is allowed, since the sudden reduction of the crystallite dimensions after this transition (to about half their values, from 700 Å to 350 Å on the average) together with the very low enthalpy involved (see above) indicate that the new phase is typically a "conformationally disordered crystal", as already observed in both organic molecules and polymers.[20] In such phases the molecules maintain the same crystal packing and unit cell dimensions, but different conformations of the side chains, owing to the relatively loose arrangement (see below).

Films cast from different solvents on to polar substrates tend to slowly crystallize into a 3D phase, with some preferred orientation along different crystallographic directions, as observed in the XRD powder patterns, where only the peaks belonging to these directions are detected. All in all, the molecules tend to stay with their conjugated residues perpendicular to the substrate.

The crystal structure of **6** consists of the packing of discrete cross-like units formed by the essentially planar conjugated backbone and by two perpendicular hexyl chains. The ORTEP drawing with labels is shown in Fig. 4. Bond distances, bond angles, and torsions, supplied as supplementary material, are quite comparable with those of **7** and dioctylfluorene.[17] In fact the hexyl-chain conformation is identical to that observed in the latter crystal, and also the fluorene moiety is planar within 0.02 Å, while the two thiophene residues, in *syn* conformations with respect to the fluorene moiety, are bent by almost 5°. The interaction between S and H(2) (short distance of 2.72 Å) allows for a planar conformation of fluorene and of the adjacent thiophene rings.

The crystal packing, reported in Fig. 5 as viewed along the *c*-axis, is composed of a network of molecules related by a four-fold alternating axis, tilted clockwise from the *a*-axis by ~25°. Each molecule, standing on a two-fold axis, is related to the nearest through contacts of the thiophene moiety with both a

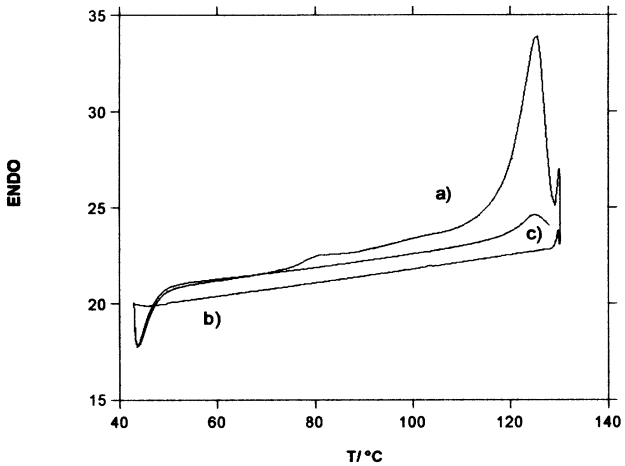

Fig. 3 DSC scans of **6** a) heating run at 20 °C min^{-1}, b) cooling run at 5 °C min^{-1}, c) second heating run at 20 °C min^{-1}.

‡CCDC reference number 158136. See http://www.rsc.org/suppdata/jm/b1/b109089p/ for crystallographic files in .cif or other electronic format.

Table 1 Crystal data of the molecules, refinement conditions and experimental details[a]

	4	**6**	**7**	**8**
Chemical formula	$C_{17}H_{14}Br_2$	$C_{32}H_{38}S_2$	$C_{25}H_{20}S_2$	$C_{29}H_{24}$
Formula weight	378.1	486.8	384.57	372.51
Space group	n°61/*Pbca*	n°88/$I4_1/a$	n° 29/$Pca2_1$	n°4/$P2_1$
a/Å	11.746(4)	16.563(1)	12.666 (4)	12.192 (8)
b/Å	11.892(3)	16.563(1)	21.383 (9)	7.217 (3)
c/Å	20.568(7)	20.657(1)	7.351 (1)	13.224 (6)
β/°				117.23(5)
V/Å^3	2873.0(16)	5666.9(5)	1990.9(16)	1034.6(17)
Z	8	8	4	2
D_{calc}/g cm^{-3}	1.748	1.14	1.28	1.20
Radiation	Cu Kα (1.54184 *λ*)		Mo Kα (0.71073 *λ*)	
μ/cm^{-1}	70.00	20.6	26.7	0.7
F(000)	1488	2144	808	396
Temperature/K	293	223	293	293
Anomalous dispersion	All non-hydrogen atoms			
Parameters refined	186	189	209	286
Unweighted agreement factor	0.033	0.041	0.061	0.062
Weighted agreement factor	0.065	0.094	0.16	0.121
Factor including unobs. data	0.070	0.091	0.19	0.166
Esd of obs. of unit weight		1.32		
Refinement	Full-matrix least-squares			
Minimization function	$\Sigma w(\|F_o\| - \|F_c\|)^2$			
Least-squares weights	$4F_o^2/\sigma^2$ (F_o^2)			
Largest shifts/*σ*	0.002	0.002	0.001	0.11
High peak in final diff. map/e Å^3	0.33(3)	0.17(3)	0.47(7)	0.17(4)
Low peak in final diff. map/e Å^3	−0.37(3)	−0.17(3)	−0.27(7)	−0.16(4)
Crystal color	White	Pale yellow	Pale yellow	White
Crystal shape	Prism	Needle	Prism	Prism
Crystal dimensions/mm^3	0.25 × 0.15 × 0.12	0.2 × 0.15 × 0.1	0.33 × 0.20 × 0.07	0.2 × 0.15 × 0.1
Instrument	Enraf-Nonius CAD4	SMART CCD	Enraf-Nonius CAD4	Enraf-Nonius CAD4
Corrections	Lorentz-polarization			
	Empirical absorption (from 1.00 to 1.01 on *I*)			
	Extinction (coefficient = 0.0000004)			
Maximum *θ*/°	69.9	23.5	27	25
Unobserved data		1084	1111	1015
Reflections included	$1617 > 2.0\sigma(F_o^2)$	967 $F_o^2 > 2.0\ \sigma(F_o^2)$	1232 with $F_o^2 > 2.0\ \sigma(F_o^2)$	959 with $F_o^2 > 2.0\ \sigma(F_o^2)$
Intensity measurements				
Monochromator	Graphite crystal, incident beam			
Attenuator	Zr foil, factor 17.0			
Detector aperture	2.0 mm horizontal		2.0 to 2.8 mm horizontal	
	4.0 mm vertical			
Scan type	*ω*–2*θ*			
Scan rate	1–20° min^{-1} (in omega)			
Scan width/deg	1.0 + 0.350 tan *θ*			

[a]Where only one value is indicated, it refers to all the crystals.

hexyl chain parallel and an aromatic residue perpendicular (edge to face contact), involving C or S atoms at distances over 3.76 Å. This relatively loose packing agrees with the low density value (1.17 g cm^{-3}), as compared with the density found in crystals of the analogous **7** (1.28 g cm^{-3}).

On the other hand, in the solvent accessible void (near −0.09, 0.01, −0.09) no relevant electronic density residue could be observed in the final difference Fourier calculation, see Table 1.

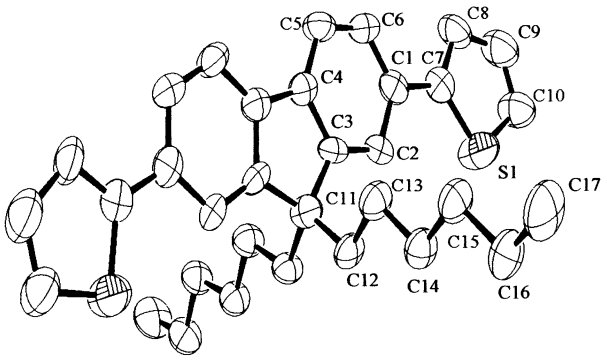

Fig. 4 ORTEP drawing of **6** with labels, the ellipsoid probability is 30%.

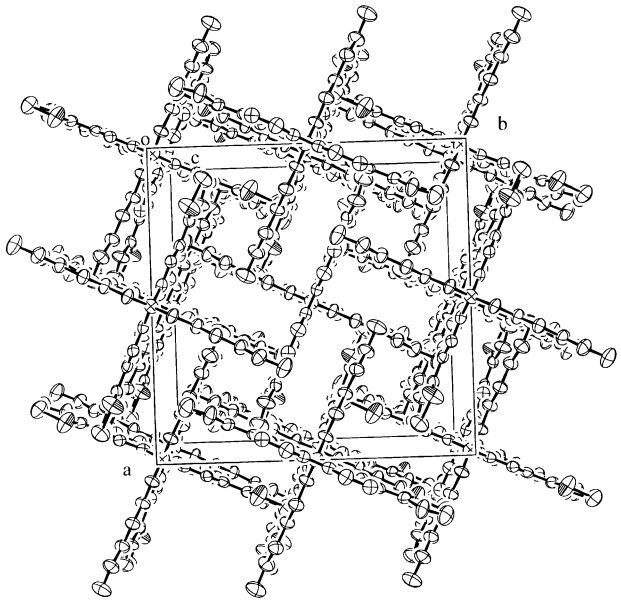

Fig. 5 Packing of the crystal of **6** , as viewed along the *c* axis. The ellipsoid probability is 25%.

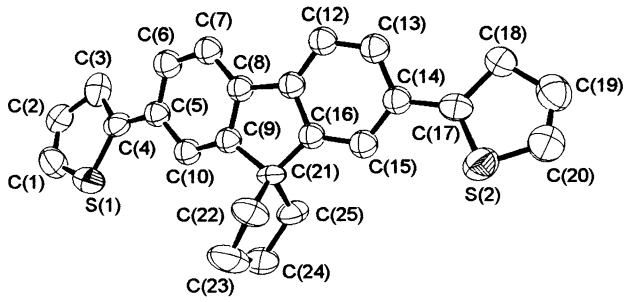

Fig. 6 ORTEP drawing of **7** and related labelling scheme. The probability of thermal ellipsoids is 30%.

Structure of 7§

The bond distances and bond angles of **7** are as expected and supplied as supplementary material. The ORTEP drawing is shown in Fig. 6.

Crystals of thiophene based oligomers, especially tetramers, often display statistical disorder in the end-thiophene groups, as first reported by Barbarella *et al.*[21] Also in this case such a disorder is present, *i.e.* the two rings predominantly assume a *syn* conformation with respect to the central cyclopentadienyl ring, which means a 180° rotation around the C(4)–C(5) and C(14)–C(17) bonds, so that atoms S(1) and S(2) replace atoms C(3) and C(18), respectively. However, since these end-residues are non-equivalent, owing to the lack of any intramolecular symmetry, the occupation factors have been refined to different values, namely 0.79 and 0.63 for atoms S(1) and S(2), respectively, with the corresponding occupancy factors of 0.21 and 0.37 for atoms C(3) and C(18), respectively.

The bond distances and bond angles of the fluorenyl residue, slightly concave, resemble those found in other parent compounds[17] and **4**, while the bent cyclopentane moiety shows the values expected considering the thermal motion. The thienyl rings present values largely affected by the statistical disorder, but attempts to refine the two sites by adopting a rigid body approach, using the geometry of oligothiophenes,[22] did not yield significant improvements. The two thiophene rings are planar within 0.022 Å and 0.012 Å respectively. Both end-thiophene rings are bent on the same side with respect to the fluorenyl mean-plane by over 24°. Also the cyclopentane moiety adopts a bent conformation, as expected.

The molecular packing, shown in Fig. 7, consists of adjacent rows of molecules strictly aligned along the *b*-axis and forming a herringbone arrangement. Each molecule forms an angle of over 65° with respect to the adjacent one. The intermolecular short contacts, close to 3.40 Å, involve atoms affected by statistical disorder, specifically atoms S(1) with C(4) ($2 - x$, $1 - y$, $\frac{1}{2} + z$) and atoms S(2) with C(14) and C(17) ($2 - x$, $-y$, $\frac{1}{2} + z$). Unlike the case of the oligothiophene series,[22,23] this peculiar packing limits π-overlap to end-thiophene moieties of adjacent molecules (see Fig. 7). This observation assumes relevance with respect to both intermolecular charge transport and energy transfer, as shown in recent studies on thiophene–phenylene oligomers,[8] in order to understand the optical properties of these molecules.

Structure of 8¶

The bond distances and bond angles of **8** are as expected and supplied as supplementary material. The ORTEP drawing with labels is shown in Fig. 8.

§CCDC reference number 158137. See http://www.rsc.org/suppdata/jm/b1/b109089p/ for crystallographic files in .cif or other electronic format.
¶CCDC reference number 158138. See http://www.rsc.org/suppdata/jm/b1/b109089p/ for crystallographic files in .cif or other electronic format.

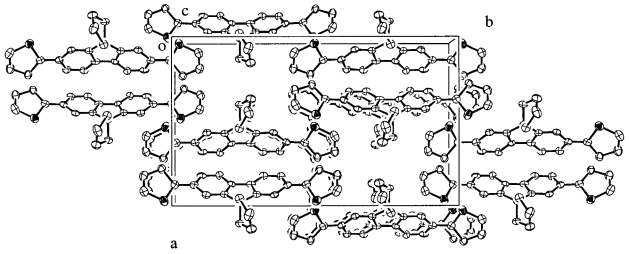

Fig. 7 Molecular packing of **7**, as viewed along the short axis.

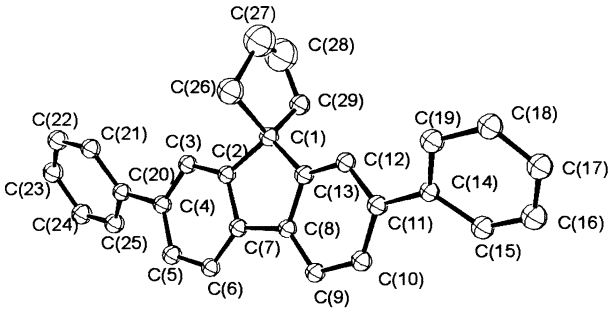

Fig. 8 ORTEP drawing of **8** and related labelling scheme. The probability of thermal ellipsoids is 25%.

The molecule crystallizes in the $P2_1$ space group and displays a high thermal motion at the end-phenyl rings at room temperature, in fact the average thermal parameters of such C-atoms together with those of the cyclopentane residue are larger than the fluorene ones, moreover a remarkable mosaic spreading in the crystal was observed; indeed the crystallization into a single crystal was critical.

On the other hand, in crystals of phenylene based oligomers, the molecules display non-planar backbone conformations,[24] and typical torsion angles close to 40°, to accommodate the steric hindrance of adjacent phenylene hydrogens; moreover the exceptional librational motion of the rings, particularly the end ones, determines a complete conformational disorder at room temperature.[25]

The bond distances and angles of the fluorene residue are comparable with those observed either in other parent compounds[17] or in crystals of **7**, while the cyclopentane moiety geometry is affected by the large thermal motion. The end-phenyl rings consequently lie out of the molecular plane of the fluorene residue by ~30° [C(14)–C(19)] and ~35° [C(20)–C(25)] respectively. The cyclopentane moiety adopts a bent conformation as observed in the crystal structure of **7**, although with very high thermal parameters.

The molecular packing, shown in Fig. 9 as viewed along the short axis, consists of overlapped layers of molecules slightly shifted relative to each other, giving thus rise to a cofacial arrangement. The intermolecular contacts, involving carbon

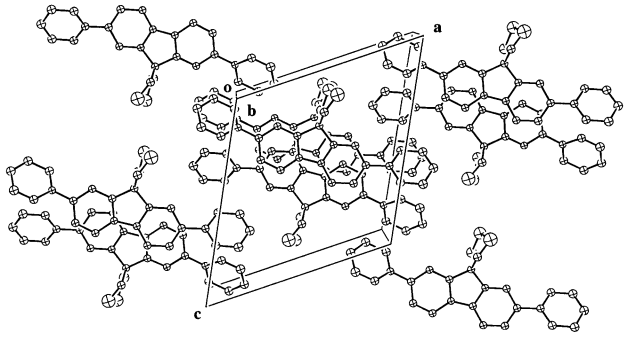

Fig. 9 Packing arrangement of **8**, as viewed along the *b* axis.

atoms are larger than 3.55 Å. However the cofacial arrangement, although partially shifted, assumed in this crystal, can guarantee an efficient π-overlap of the adjacent faced molecules.[8]

Optical studies

The influence of the addition of electron donation (thienyl group) or electron withdrawal (benzonitrile group) to/from the fluorene core on the absorption and emission properties is clearly shown in Table 2, where the absorption and emission maxima of $CHCl_3$ and THF solutions respectively of the oligomers are reported. The effect of thienyl substitution on a fluorene core is a clear red-shift with respect to the phenyl addition, while a *p*-nitrilo group produces a blue-shift with respect to **8**, especially for the emission. This observation is accounted for considering that the electron withdrawing mesomeric effect of the cyano group is more effective in the excited planar state of the molecule.

Table 2 also reports the photoluminescence quantum yields (PL-QY) values for diluted THF solutions, the energy gap (EG) values for cast films, the corresponding oxidation potentials and electronic affinities calculated according to ref. 26. The QY measurements are carried out in very dilute ($\sim 10^{-5}$ M) solutions, particularly for **9** (10^{-6} M) because of its strong tendency to aggregate producing a sharp decrease of PL intensity even in 10^{-5} M solution (QY $\approx$ 8%).

Absorption and PL investigations are performed in the solid state for cast films and single crystals, for **6**, **7**, and **8**; PL of **7** and **8** vacuum evaporated films are also measured.

While all the molecules display noticeable PL in solution, in solid state a selective reduction is detected, particularly for **9**.

In Fig. 10 the optical spectra of **8**, which is treated first as it has the lowest PL in the series, are reported. The absorption spectrum of the cast film displays a long wavelength shoulder at about 350 nm, that is not present in the spectrum of the solution. The PL spectra of the cast films are quite different from those of the solution. In fact, while for the solution a structured spectrum, peaking at 352 nm, is observed, the solid state samples display an unstructured, red-shifted band, peaking at 404 nm (cast film) and 420 nm (single crystal). The PL spectrum of the vacuum evaporated films, with a maximum at 380 nm, shows a smaller red-shift, with respect to the solution spectrum, which increases in time by leaving the evaporated film in air or under nitrogen atmosphere, at room temperature. Moreover, as shown in Fig. 10, by ageing the film, the PL intensity decreases and a long wavelength component at about 540 nm appears.

In Fig. 11 and Fig. 12 the optical spectra of **7** and **6** respectively are reported. The introduction of thienyl end-groups instead of phenyls induces a red-shift of the absorption and emission spectra of **6** and **7** solutions, with respect to those of **8**. On the other hand, the change of the alkyl substituent at the 9-position gives no modification of the optical properties. In fact, the spectra of diluted solutions of **6** and **7** are very similar. Indeed **7** solutions show a higher tendency to aggregate at high concentrations and, as can be seen in Fig. 11, concentrated (10^{-2} M) solutions of molecule **7** display absorption and PL spectra similar to those of the cast films.

Cast films of both **6** and **7** oligomers show absorption and

Table 2 Optical and electronic data for the oligomers

Molecules	Absorption/ nm	Emission/ nm	PL-QY (%)	EG/ eV	E_{ox}/ V	EA/ eV
Fluorene	260[a]	290	—	—	—	—
6	353	382	65	3.05	0.85	2.2
7	354	382	55	3.11	0.8	2.09
8	326	353	45	3.16	1.05	2.29
9	319	323	60	3.03	—	—

[a]Cyclohexane solution.

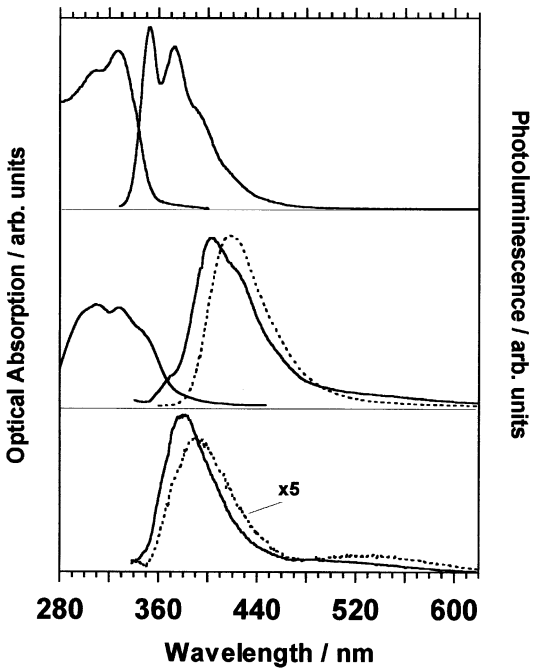

Fig. 10 Optical absorption and emission spectra of **8**. Top: diluted THF solution; middle: cast films (solid line) and single crystal (dotted line); bottom: vacuum evaporated film as prepared (solid line) and after 10 days ageing (dotted line).

PL spectra only slightly red-shifted with respect to the solutions. Moreover, after heating (140 °C) and fast quenching of the cast film of **6**, both its absorption and structured PL component show exactly the same shape and spectral position observed in the diluted solution spectra.

The emission of the single crystals is red-shifted with respect to the PL of the cast and evaporated films, for all three molecules. In this respect, it should be mentioned that, following Cornil *et al.*,[8] the tight crystal packing of molecules

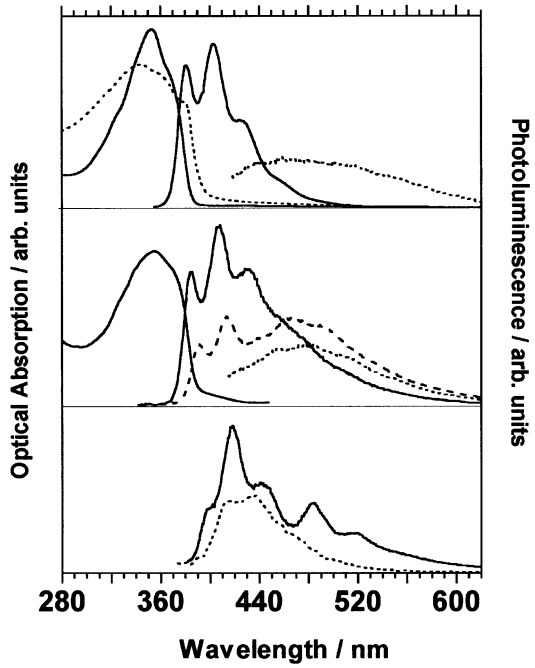

Fig. 11 Optical absorption and emission spectra of **7**. Top: diluted (solid line) and concentrated (dotted line) THF solution excited at 340 nm and 410 nm, respectively; middle: cast film excited at 340 nm (solid line) and 400 nm (dotted line) and cast film after degradation (dashed line); bottom: vacuum evaporated film (solid line) and single crystal (dotted line).

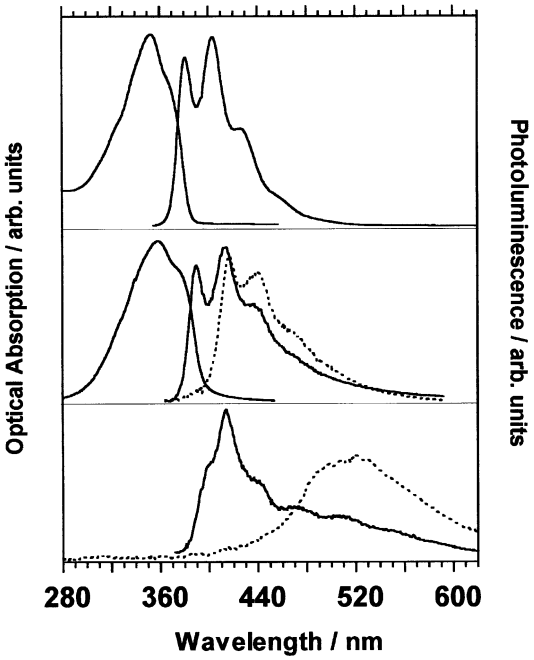

Fig. 12 Optical absorption and emission spectra of **6**. Top: diluted THF solution; middle: cast film (solid line) and single crystal (dotted line); bottom: PL (solid line) and EL (dashed line) of spin coated film (see text).

7 and **8** should induce a drastic quenching of the photoluminescence, hence the grain-boundary defects of the small single crystals, here studied, could likely act as emission centers.[27] In contrast, the crystal packing of molecules of **6**, where the distance between adjacent molecules is close to 8 Å, should allow for intrinsic emission. However, to definitely assess the intrinsic PL-QY of the molecules an accurate measurement on single crystals is in progress.

The presence of a broad low energy tail in the PL spectra of the cast films suggests that both the amorphous (structured blue component of the spectra, similar to the solution) and the crystalline phase (broad low energy shoulder, similar to the single crystal) are present in the cast films. In particular, for cast films of **6**, the intensity of the low energy component increases, with respect to the structured blue component, after only few days ageing, indicating a strong tendency to self-crystallization of this molecule. This phenomenon clearly appears in thin spin-coated and cast films of **6** which lose their transparency in about 1–2 days.

The PL of the cast films of **6** and **7** display an additional low energy broad component in the 420–520 nm region, which can be selectively obtained by exciting at wavelengths above 400 nm, and is particularly evident in films of **7** (see Fig. 11). This component is also observed in concentrated solutions of **7** (see Fig. 11), disappearing on successive dilution. The same broad component is observed to increase in intensity, with respect to the structured component, in cast films after prolonged exposure to light and air, or after thermal annealing in vacuum or in air. In Fig. 11 the PL spectrum of a cast film of **7** is shown for a sample heated in air under light exposure. This low energy component is also observed in evaporated films, displaying a well structured emission with peaks at 485 and 520 nm. In these samples we do not detect any evidence for chemical degradation as no signals attributable to oxygen derivatives could be detected either in ^{1}H NMR or FTIR analysis. This low energy component seems thus to be associated with aggregation rather than degradation effects. Similar observations on polyfluorenes have been reported by Miller *et al.*[5,28] and have been attributed to aggregate formation. PL-QY of cast films are not reported due to the different tendencies towards crystallization/aggregation of the molecules, which prevent any quantitative measurement.

On the basis of these findings some insights on the nature of aggregates can be suggested, namely a few molecules (two or three) approaching face to face, therefore realising efficient π-overlap, unlike the 3D structure (see above). Such short-range order, undetectable by structural investigations,[29] is likely developed from amorphous regions and is responsible for the low energy emission. This organization is different from both that of amorphous regions, where no translational order is achieved, and that of crystalline regions, where long range order is detected.[29]

In conclusion, in the solid state quite different absorption and PL spectra are observed, depending on the aggregation type attained and on the ageing of the samples. Different PL emissions are assigned to contributions from the amorphous, the crystalline and the aggregated components of the samples indicating a progressive shift towards lower energy by passing from disordered (partially amorphous) cast films to crystalline samples, and from crystalline films to aggregated samples. While films of **6** display a high tendency to self-crystallization, cast films of **7** , as well as cast and evaporated films of **8**, appear to be more sensitive to aggregation effects spontaneously occurring by ageing the samples.

Electroluminescence (EL) was not observed in **6**, **7** and **8** single-layer devices using ITO and Al as electrodes. Even the use of Ca instead of Al as cathode did not allow the observation of any emission from a device with a spin coated film of **7** as active layer. On the contrary the ITO/**6**/Ca–Al device yielded a green emission, at high applied voltages (20–30 V) with low current densities (0.8–2 10^{-3} A cm^{-2}) with a maximum efficiency of about 4×10^{-2}%. The spectral position of electroluminescence of **6** is reported in Fig. 12 together with the PL obtained from the same film. The low energy position of the EL spectrum can be attributed to aggregate emission of the material at the metal interface, where electron–hole recombination takes place. In fact the spectral shape of the PL obtained by exciting the film from the ITO interface of the device, after device operation, resembles that of the crystalline phase with an additional low energy component (similar to that observed in the PL after thermal annealing or ageing of the films). The film region at the cathode interface can undergo softening by heating during metal deposition, see DSC analysis. The reason for the low currents observed can be found in the high tendency of films of **6** to crystallize. Indeed, considering the structural results, it is expected that the peculiar packing of crystalline **6** does not favour an efficient charge transport. All in all, the EL study indicates that, even though the work function of the electrodes matches well with both ionization potential and electronic affinity of the oligomers (see Table 2 and ref. 30) and fluorene derivatives are expected easily to inject electrons from Ca rather than holes from ITO electrodes,[31] the high tendency of **6** to crystallize reduces the charge mobility in the material thus limiting the potential of this material in LED fabrication.

Conclusions

Fluorene core oligomers with thienyl and phenyl end groups have been synthesized *via* organometallic synthesis, then characterized both optically and structurally. The noticeable PL of all the compounds in solution is modulated in solid state. A comparison among the crystal structures of three oligomers possessing different crystal packings can be performed by considering the mean distances calculated between the closest faced conjugated residues, which vary from 4.9 Å, in crystal **8**, to 5.1 Å, in **7**, up to about 8 Å, in **6**. Such facing between adjacent molecules is more efficient for **8**, while in **7** a displaced herringbone type of arrangement is observed and in **6** a very far shifted facing is detected. Indeed many factors contribute

to the solid state PL-QY,[5–8] but the packing features are insufficient to establish a ranking in the series; in this respect further studies have to be performed.

The dependence of the optical properties of the three molecules on their state of aggregation and its time evolution have been reported. In diluted solutions, the PL-QY values range from 45% to 65%. Absorption and emission spectra of thienyl-residue containing molecules are red-shifted. In the oligomer having linear alkyl chains as substituents, a quite fast progressive crystallization takes place, while for molecule **7** the solid state arrangement does not appreciably modify in short times at room temperature. A progressive red-shift of the PL is observed in the solid state by passing from amorphous films (cast films or vacuum evaporated films) to crystals, to aggregated films. Freshly prepared vacuum evaporated films of **7** and **8** display spectra similar to those of amorphous samples and are quite sensitive to aggregation effects during time. The features of the amorphous component mainly are observed in cast or spin coated films from solution of **6** and **7**. In contrast, cast films of **8** give rise to an emission similar to that of the crystalline phase, due to both crystal defects and large mosaic spread. The study of a single layer LED device of **6** indicates that the strong tendency of the film to crystallize induces very low charge mobility giving electroluminescence spectra typical of the aggregated material at the metal interface.

Experimental

Materials

Fluorene (Aldrich), bromine (Merck), butyllithium 1.6 M in hexane and *tert*-butyllithium 1.7 M in pentane, 1,4-dibromobutane and 1-bromohexane, 4-bromobenzonitrile (Aldrich) and $Pd(PPh_3)_4$ (Janssen) were used as received. All the solvents tetrahydrofuran (THF), diethyl ether, toluene, were freshly distilled. 2-Isopropoxy-4,4,5,5-tetramethyl-1,3,2-dioxaborolane obtained from Aldrich was stored under nitrogen.

9,9-Dihexylfluorene (1)

7.87 ml (12.6 mmol) of *n*-butyllithium were added dropwise during 20 min to a stirred solution of fluorene 1 g (6 mmol) in THF (14 ml) at −78 °C; the colour of the solution became red-orange. The mixture was stirred at −78 °C for 45 min and 1.94 ml (13.8 mmol) of hexyl bromide in THF (3 ml) were added dropwise during 20 min. The solution was allowed to warm to room temperature and stirred for 3 h. The mixture was poured into water, which bleached the colour, and extracted with ether. The organic extracts were washed with brine and dried over magnesium sulfate, and the solvent was removed by a rotary evaporator to provide 1.98 g (yield 99%) of the title compound as a white, deliquescent solid. Mp 30–32 °C; MS(EI): m/z = 334 [M^+]; FTIR (cm^{-1}): 1450, 760, 730; ^{1}H-NMR (500 MHz, $CDCl_3$, ppm) 7.79 (dd, 4 and 5 protons, J_o = 6.8 Hz, J_m = 1 Hz), 7.43 (dd, 1 and 8 protons, J_o = 7.0 Hz, J_m = 1.1 Hz), 7.39 (overlapped triplets, protons 2, 3 and 6, 7, J_o = 7.5 Hz), 2.08–205 (m, 4H, α methylene protons), 1.23–1.14 (m, 12H), 0.86 (t, 6H, methyl protons, J = 7.17 Hz), 0.77 (m, 4H, β methylene protons).

2,7-Dibromo-9,9-dihexylfluorene (2)

The reaction was carried out in the dark to avoid bromination of the aliphatic chains. To a stirred solution of 9,9-dihexylfluorene 0.79 g (2.38 mmol) in $CHCl_3$ (3.6 ml) at 0 °C, 4.86 g (0.03 mmol) of ferric chloride and 0.25 ml (4.98 mmol) of bromine were added. The red solution was allowed to warm to room temperature and stirred for 3 h. The resulting slurry was poured into water and washed with sodium thiosulfate until the colour disappeared. The organic layer was dried over magnesium sulfate and the solvent was removed under reduced pressure to give a pale yellow oil. Recrystallization in hexane afforded 0.88 g of white crystals (yield 75%). Mp 67.5–68.5 °C; MS(EI): m/z = 492 [M^+]; FTIR (cm^{-1}): 1468, 1070, 880, 810; ^{1}H-NMR (270 MHz, $CDCl_3$, ppm): 7.52 (d, 4 and 5 protons, J_o = 6.6 Hz,), 7.45 (dd, 3 and 6 protons, J_o = 6.6 Hz, J_m = 1.7 Hz), 7.44 (d, protons 1 and 8, J_m = 1.7 Hz), 1.94–1.88 (m, 4H, α methylene protons), 1.19–1.03 (m, 12H), 0.78 (t, 6H, methyl protons, J = 6.91 Hz), 0.64–0.52 (m, 4H, β methylene protons).

Spiro[cyclopentane-1,9′-fluorene] (3)

4 ml (6.3 mmol) of *n*-butyllithium were added dropwise during 15 min to a stirred solution of 0.5 g (3 mmol) of fluorene in THF (14 ml) at −78 °C in the dark; the colour of the solution became orange. The mixture was stirred at −78 °C for 45 min and then diluted with THF (14 ml), and then a solution of 0.65 g (3 mmol) of 1,4-dibromobutane in THF (3 ml) was added dropwise during 10 min. The solution was allowed to warm to room temperature, then it was stirred for 4 h. The mixture was poured into water, which caused bleaching of the colour, and extracted with ether. The organic layers were washed with brine and dried over magnesium sulfate; the solvent was removed by a rotary evaporator. The crude white solid was washed with EtOH to provide 0.65 g (99%) of the title compound as a white waxy solid. Mp 88–90 °C; MS (EI): m/z = 220 [M^+]; FTIR (cm^{-1}): 1468, 760, 732; ^{1}H-NMR (270 MHz, $CDCl_3$, ppm) 7.71–7.68 (m, protons 4 and 5 which are non-equivalent), 7.45–7.41 (m, protons 1 and 8), 7.32–7.28 (m, 4H, protons 2,3,6 and 7), 2.17–2.04 (m, 8H, aliphatic protons).

2′,7′-Dibromospiro[cyclopentane-1,9′-fluorene] (4)

The bromination was carried out in the dark. 3.2 mg (0.017 mmol) of ferric chloride and 0.17 ml (3.3 mmol) of bromine were added to a stirred solution of 0.34 g (1.57 mmol) of spiro[cyclopentane-1,9′-fluorene] in $CHCl_3$ (2.4 ml) at 0 °C. The solution was allowed to warm to room temperature and stirred for 4.30 h. The resulting slurry was poured into water and washed with sodium thiosulfate until the colour disappeared. The organic layer was dried over magnesium sulfate to give of a pale yellow oil which was recrystallized in hexane to afford 0.5 g of white crystals (yield 85%). Mp 164.5–166.5 °C; MS (EI): m/z = 378 [M^+]; FTIR (cm^{-1}): 1468, 1212, 886, 820; ^{1}H-NMR (270 MHz, $CDCl_3$, ppm) 7.53 (d, protons 1 and 8, J_m = 1.5 Hz), 7.51 (d, protons 4 and 5, J_o = 8.1 Hz), 7.44 (dd, protons 3 and 6, J_o = 8.1 Hz, J_m = 1.5 Hz), 2.16–2.03 (m, 8H, aliphatic protons).

2′,7′-Bis(4,4,5,5-tetramethyl-1,3,2-dioxaborolan-2-yl)spiro[cyclopentane-1,9′-fluorene] (5)

To a solution of 200 mg (0.52 mmol) of 2′,7′-dibromospiro-[cyclopentane-1,9′-fluorene] in dry THF (8 ml) at −78 °C was added dropwise *n*-butyllithium (0.7 ml, 0.52 mmol). The greenish blue mixture was stirred at this temperature during 1 h and 30 min, then 2-isopropoxy-4,4,5,5-tetramethyl-1,3,2-dioxaborolane (298 mg, 1.82 mmol) was added by syringe, and the resulting solution was stirred at −78 °C for 1 h. In that time the colour changed from brown through red to orange, then the bath was left to reach room temperature very slowly under stirring during 24 h. The pale yellow mixture was poured into water and extracted with ether. The organic layer was washed with water, brine and dried over $MgSO_4$. After removal of the solvent, preparative TLC (hexane : ethyl acetate, 93 : 7 as eluent) gave 38 mg of the title compound as a pale yellow solid (yield 15%) MS (EI): m/z = 472 [M^+]; ^{1}H-NMR (500 MHz, $CDCl_3$, ppm) 7.86 (s, protons 1 and 8), 7.79 (d, protons 4 and 5, J_o = 7.52 Hz), 7.72 (d, protons 3 and 6, J_o = 7.52 Hz,), 2.17–2.10 (m, 8H, aliphatic protons), 1.36 (s, 24H, methyl protons).

2,7-Di(2-thienyl)-9,9-dihexylfluorene (6)

2,7-Dibromo-9,9-dihexylfluorene (0.19 g, 0.33 mmol), Pd-(PPh_3)$_4$ (44 mg, 0.038 mmol) and 2-tributylstannylthiophene (0.32 g, 0.85 mmol) were dissolved in 3 ml of dry toluene. The reaction was performed following the procedure reported above for 2′,7′-di(2-thienyl)spiro[cyclopentane-1,9′-fluorene] except for the recrystallization from toluene–hexane mixture giving the title compound as a pale yellow solid (yield 57%). Mp 122 °C; MS (EI): m/z = 498 [M^+]; ^{1}H-NMR (270 MHz, $CDCl_3$, ppm) 7.68 (d, protons 4 and 5, J_o = 7.9 Hz), 7.60 (dd, protons 3 and 6, J_o = 7.9 Hz, J_m = 1.6 Hz), 7.56 (d, protons 1 and 8, J_m = 1.6 Hz), 7.38 (dd, 2H, 3′ thienyl proton, $J_{3',4'}$ = 3.6 Hz, $J_{3',5'}$ = 1.1 Hz), 7.29 (dd, 2H, 5′ thienyl proton, $J_{5',4'}$ = 5.1 Hz, $J_{3',5'}$ = 1.1 Hz), 7.1 (dd, 2H, 4′ thienyl proton, $J_{4',5'}$ = 5.1 Hz, $J_{4',3'}$ = 3.6 Hz), 2.04–1.98 (m, 4H, α methylene protons), 1.38–1.21 (m, 4H, γ methylene protons), 0.91 (t, 6H, methyl protons, J = 7.21 Hz), 0.83–0.69 (m, 4H, β methylene protons). Elemental analysis for $C_{33}H_{38}S_2$ (%): calculated C 79.45; H 7.68; S 12.86; found C 79.52; H 7.73; S 12.45.

2′,7′-Di(2-thienyl)spiro[cyclopentane-1,9′-fluorene] (7)

2′,7′-Dibromospiro[cyclopentane-1,9′-fluorene] (0.15 g, 0.4 mmol) and Pd(PPh_3)$_4$ (45 mg, 0.04 mmol) were dissolved in 3 ml of dry toluene. After the addition of 2-tributylstannylthiophene (0.32 g, 0.85 mmol) the solution was heated at 55 °C for 1 h and at 105 °C overnight, then it was poured into 5 ml of 2 M HCl. The aqueous layer was extracted many times with toluene. All the organic phases were collected, neutralized with $NaHCO_3$ and water, then dried over Na_2SO_4. The crude solid resulting from solvent removal was purified by flash chromatography using heptane : dichloromethane (7 : 3) giving the title compound as a pale yellow solid (yield 72%). Mp 181.7–182.7 °C; MS (EI): m/z = 384 [M^+]; FTIR (cm^{-1}) 1596, 1468, 1414, 888, 816, 760, 700; ^{1}H-NMR (270 MHz, dTCE, ppm) 7.69 (d, 2H, protons 4 and 5, J_o = 7.9 Hz), 7.59 (dd, 2H, protons 3 and 6, J_o = 7.9 Hz, J_m = 1.1 Hz), 7.64 (s, 2H, protons 1 and 8), 7.38 (d, 2H, 3′ thienyl proton, $J_{3',4'}$ = 3.7 Hz), 7.31 (d, 2H, 5′ thienyl proton, $J_{5',4'}$ = 5.0 Hz), 7.12 (dd, 2H, 4′ thienyl proton, $J_{4',5'}$ = 5.0 Hz, $J_{4',3'}$ = 3.7 Hz), 2.20–2.14 (m, 8H, aliphatic protons). Elemental analysis for $C_{25}H_{20}S_2$ (%): calculated C 78.08; H 5.24; S 16.68; found C 78.15; H 5.29; S 16.49.

2′,7′-Diphenylspiro[cyclopentane-1,9′-fluorene] (8)

To a solution of bromobenzene (0.1 g, 6.37 mmol) in diethyl ether (8 ml), *tert*-butyllithium (13.3 mmol) dissolved in Et_2O (4 ml) was added dropwise during 15 min at −78 °C. The solution was stirred at −78 °C for 1 h and transferred *via* cannula into anhydrous zinc chloride (1.22 g, 8.95 mmol) dissolved in THF (8 ml) at room temperature. The resulting slurry was stirred for 1 h at room temperature, than was transferred by cannula into a round flask containing Pd(PPh_3)$_4$ (13.7 mg, 0.012 mmol) and 2′,7′-dibromospiro[cyclopentane-1,9′-fluorene] (300 mg, 0.79 mmol) in THF (4.5 ml). The pale yellow solution was heated to 55 °C and became brown during stirring for 16 h; then it was cooled to room temperature and poured into water. The aqueous layer was extracted three times with $CHCl_3$ and the collected organic layers were washed with 3 M HCl, water and dried over Na_2SO_4. The crude pale yellow solid resulting from solvent removal was washed several times with pentane then it was crystallized from toluene–ethanol mixture giving 0.23 g of the title compound as a white solid (yield 77%). Mp 219–221 °C; MS (EI): m/z = 372 [M^+]; FTIR (cm^{-1}): 1596, 1464, 888, 816, 760, 700; ^{1}H-NMR (500 MHz, CD_2Cl_2, ppm) 7.78 (d, 2H, protons 4 and 5, J_o = 7.8 Hz), 7.69–7.65 (m, 6H), 7.59 (d, 2H, protons 3 and 6, J_o = 7.8 Hz), 7.47 (dd, 4H, *m*-protons in phenyl ring, J_o = 7.52), 7.37 (t, 2H, *p*-proton in phenyl ring, J_o = 7.22 Hz), 2.19 (s, 8H, aliphatic protons). Elemental analysis for $C_{29}H_{24}$ (%): calculated C 93.51; H 6.49; found C 93.43; H 6.54.

2′,7′-Bis(4-cyanophenyl)spiro[cyclopentane-1,9′-fluorene] (9)

4-Bromobenzonitrile (29.5 mg, 0.19 mmol), 2′,7′-bis(4,4,5,5-tetramethyl-1,3,2-dioxaborolan-2-yl)spiro[cyclopentane-1,9′-fluorene] (38 mg, 0.08 mmol) and Pd(PPh_3)$_4$ were dissolved in a mixture of toluene (2 ml) and aqueous 2 M Na_2CO_3 (1.4 ml) under nitrogen atmosphere. The solution was refluxed during 25 h, than poured into slightly acid (HCl) water and extracted more times with ether. The collected organic phase was dried over Na_2SO_4 and the solvent removed. Purification was performed on preparative TLC (hexane : ethyl acetate, 93 : 7 as eluent) yielding a white solid (60%). Mp 343–344 °C; MS (APCI): m/z = 423 [M+H]$^+$; ^{1}H-NMR (500 MHz, $CDCl_3$, ppm) 7.83 (d, protons 4 and 5, J_o = 7.9 Hz), 7.75 (s, 8H, end-phenyl protons), 7.65 (d, protons 1 and 8, J_m = 1.4 Hz), 7.59 (dd, protons 3 and 6, J_o = 7.9 Hz, J_m = 1.4 Hz), 2.21 (s, 8H, aliphatic protons). Elemental analysis for $C_{31}H_{22}N_2$ (%): calculated C 88.12; H 5.25; N 6.63; found C 88.09; H 5.22; N 6.65.

Methods

Mass spectrometric measurements were performed on a Hewlett Packard 5985 B GC-MS instrument equipped with a DB-5 MS (30 m) capillary column. Mass spectral data were obtained under the following conditions: ionizing energy, 70 eV; ion source temperature, 200 °C; GC/MS transfer line temperature, 280 °C; scanning rate 1.2 scans s^{-1} over the mass range m/z = 33–520. Molecules of **9**, introduced by direct injection, were detected with a Finnigan MAT LCQ ion trap mass spectrometer operating in APCI(+) mode. ^{1}H-NMR spectra were recorded on either a Bruker DMX 500 or a 270 MHz spectrometer. Absorption UV–vis spectra were obtained either in $CHCl_3$ or in cyclohexane using a Varian-Cary 2400 instrument. Fluorescence emission spectra were obtained from THF solutions with the help of a SPEX 270M polychromator equipped with a cooled CCD detector by exciting with a Xenon lamp. PL-QY in solution was measured by using quinine sulfate as a reference, in diluted solution ($<10^{-5}$ M).

FTIR-spectra were recorded on a Bruker IFS 48 instrument. Melting points were obtained by using either a Reichert microscope coupled with a Mettler FP5 hot stage or a DSC Perkin-Elmer PYRIS1 apparatus. All XRD experimental details, structural resolution and refinement of the four crystal structures are reported in Table 1. XRD patterns of powders and films were obtained using a computer controlled Siemens D-500 diffractometer equipped with an Anton-Paar camera for variable temperature experiments under nitrogen atmosphere.

The structures were solved by direct methods using the SIR88 program for **7** and **8** and SIR92 program for **4** and **6**.[32] Refinement using full-matrix least-squares was carried out keeping the hydrogen atoms fixed to the corresponding C-atoms at 0.95 Å, with the same isotropic thermal parameters multiplied by 1.3. In view of its ease of crystallization, **8** displays twinned crystals and over more than 50 samples examined, the only single crystal was of insufficient quality, in fact a large mosaic dispersion was detected; this accounts for the very approximate crystal structure obtained, see Table 2. A list of the observed and calculated structure factors together with torsion angles and anisotropic thermal vibration parameters is available on request to the authors.

All reactions were carried out under an atmosphere of purified inert gas, *i.e.* nitrogen. Flash chromatography was performed on silica gel 60, 230–400 mesh ASTM (Merck or Macherey-Nagel) column.

Film and device preparation

Thin films of **6** and **7**, up to 400 Å thick, were prepared by vacuum deposition at 10^{-7} mbar, using a double filament Knudsen cell, heating the crucible at the optimized evaporation temperature of 185 °C and 175 °C respectively, after a slow heating ramp suitably chosen to prevent overheating of the source. The mean growing rates ranged from 3 Å min^{-1} to 5 Å min^{-1}.

Cast films of **6**, **7**, **8**, **9** were obtained on quartz and ITO at room temperature from THF, $CHCl_3$, cyclohexane and toluene. Subsequent thermal treatments on films of **6** were carried out under nitrogen atmosphere, after three evacuation cycles.

Spin coated films of **6** were prepared at 2000 rpm from cyclohexane and toluene solution (8 mg cm^{-3}). Very thin films ($A < 0.05$) were used for PL measurements, while thicker films were employed for device preparation. LEDs were prepared by spin coating onto ITO (indium–tin-oxide) coated glass substrates, by evaporating Ca and Al as top electrode at vacuum $<10^{-6}$ mbar and deposition rates of 150 Å min^{-1}.

Acknowledgement

Partial contributions to this work from both oriented project MATSTA II of C.N.R. and project "Nanotechnologies" of M.U.R.S.T. are kindly acknowledged. We also thank Professor Lanfranchi for useful discussions. We are also indebted to Professor F. De Martin of "Dipartimento di Chimica Strutturale e Stereochimica Inorganica" for single crystal structural analysis.

References

1 *e.g.* C. Ziegler, in *Handbook of Organic Conductive Molecules and Polymers*, ed. H. S. Nalwa, J. Wiley & Sons, Chichester, 1997, vol. 3, p. 677.
2 *e.g.* G. Leising, S. Tasch and W. Graupner, in *Handbook of Conductive Polymers*, ed. T. A. Skotheim, R. L. Elsenbaumer and J. R. Reynolds, M. Dekker, New York, 1998, p. 847.
3 J. Roncali, *Chem. Rev.*, 1997, **97**, 173; Y. Shirota, *J. Mater. Chem.*, 2000, **10**, 1.
4 S. H. Lee and T. Tsutsui, *Thin Solid Films*, 2000, **363**, 76; G. Klaerner and R. D. Miller, *Macromolecules*, 1998, **31**, 2007.
5 M. Kreyenschmidt, G. Klaerner, T. Fuhrer, J. Ashenhurst, S. Karg, W. D. Chen, V. Y. Lee, J. C. Scott and R. D. Miller, *Macromolecules*, 1998, **31**, 1099.
6 Q. Pei and Y. Yang, *J. Am. Chem. Soc.*, 1996, **118**, 7416; M. Grell, D. D. C. Bradley, M. Inbasekaran and E. P. Woo, *Adv. Mater.*, 1997, **9**, 798; X. Long, A. Malinowski, D. D. C. Bradley M. Imbasekaran and E. P. Woo, *Chem. Phys, Lett.*, 1997, **272**, 6; H. N. Cho, J. K. Kim, C. Y. Kim, N. W. Song and D. Kim, *Macromolecules*, 1999, **32**, 1476; B. Tsuie, J. L. Reddinger, G. A. Sotzing, J. Sodolucho, A. R. Katritzky and J. R. Reynolds, *J. Mater. Chem.*, 1999, **9**, 2189; A. Donat-Bouillud, I. Lévesque, Y. Tao, M. D'Iorio, S. Beaupré, P. Blondin, M. Ranger, J. Bouchard and M. Leclerc, *Chem. Mater.*, 2000, **12**, 1931; M. Bernius, M. Inbasekaran, E. Woo, W. Woo and L. Wujkowski, *Thin Solid Films*, 2000, **363**, 55.
7 M. Grell, D. D. C. Bradley, M. Imbasekaran and E. P. Woo, *Adv. Mater.*, 1997, **9**, 798; E. P. Woo, W. R. Shiang, M. Imbasekaran and G. R. Roof, *US Patent* 5708130, 1998; M. Grell, W. Knoll, D. Lupo, A. Meisel, T. Miteva, D. Neher, H. Nothofer, U. Scherf and A. Yasuda, *Adv. Mater.*, 1999, **11**, 671; A. E. A. Contoret, S. R. Ferrer, P. O. Jackson, S. M. Khan, L. May, M. O'Neill, E. Nicholls, S. M. Kelly and J. C. Richards, *Adv. Mater.*, 2000, **12**, 971.
8 J. Cornil, D. A. dos Santos, X. Crispin, R. Silbey and J. L. Brédas, *J. Am. Chem. Soc.*, 1998, **120**, 1289; J. Cornil, J. Ph. Calbert, D. Beljonne, R. Silbey and J. L. Brédas, *Adv. Mat*, 2000, **12**, 978; J. Cornil, J. Ph. Calbert and J. L. Brédas, *J. Am. Chem. Soc.*, 2001, **123**, 1250.
9 M. Belletête, J. F. Morin, S. Beauprè, M. Ranger, M. Leclerc and G. Durocher, *Macromolecules*, 2001, **34**, 2288.
10 N. Johansson, D. A. Dos Santos, S. Guo, J. Cornil, M. Fahlman, J. Salbeck, H. Schenk, H. Arwin, J. L. Brédas and W. R. Salanek, *J. Chem. Phys.*, 1997, **107**, 2542; R. W. Alder, K. R. Anderson, P. A. Benjes, C. P. Butts, P. A. Kouitentis and A. G. Orpen, *Chem. Commun.*, 1998, 309; N. Johansson, J. Salbeck, J. Bauer, F. Weissörtel, P. Bröms, A. Andersson and W. R. Salaneck, *Adv. Mater.*, 1998, **10**, 1136; W. Kreuder, D. Lupo, J. Salbeck, H. Schenk and T. Stehlin, *US Patent* 5621131, 1997; D. Lupo, J. Salbeck, H. Schenk, T. Stehlin and R. Stern, U. S. Patent 5840217, 1998; W. Yu, J. Pei and A. J. Heeger, *Adv. Mater.*, 2000, **12**, 828.
11 M. Fukuda, M. Sawada and K. Joshino, *J. Polym. Sci., Part A: Polym. Chem.*, 1993, **31**, 265.
12 M. Ranger, D. Rondeau and M. Leclerc, *Macromolecules*, 1997, **30**, 7686.
13 J. K. Stille, D. R. McKean, G. Parrinello and A. F. Renaldo, *J. Org. Chem.*, 1987, **52**, 422.
14 F. Larmat, J. R. Reynolds, B. A. Reinhardt, L. L. Brott and S. J. Clarson, *J. Polym. Sci., Part A: Polym. Chem.*, 1997, **35**, 3627.
15 M. Ranger and M. Leclerc, *Chem. Comm.*, 1997, 1491; M. Ranger and M. Leclerc, *Can. J. Chem.*, 1998, **76**, 1571.
16 N. Miyaura and A. Suzuki, *Chem. Rev.*, 1995, **95**, 2457.
17 M. Leclerc, M. Ranger and F. Bélanger-Gariépy, *Acta Crystallogr., Sect. C*, 1998, **54**, 799.
18 H. F. Lieberman, R. J. Davey and D. T. M. Newsham, *Chem. Mater.*, 2000, **12**, 309.
19 A. Bolognesi, W. Porzio, G. Zhuo and T. Ezquerra, *Eur. Polym. J.*, 1996, **32**, 1097.
20 B. Wunderlich, M. Moeller, J. Grebowicz and H. Baur, *Adv. Polym. Sci.*, 1998, **87**, 1.
21 G. Barbarella, M. Zambianchi, A. Bongini and L. Antolini, *Adv. Mater.*, 1993, **5**, 834.
22 W. Porzio, S. Destri, M. Mascherpa and S. Brückner, *Acta Polym.*, 1993, **44**, 266.
23 D. Fichou, B. Bachet, F. Demanze, I. Billy, G. Horowitz and F. Garnier, *Adv. Mater.*, 1996, **8**, 500.
24 K. Baker, A. Fratini, T. Resch, H. Knachel, W. Adams, E. Socci and B. Farmer, *Polymer*, 1993, **34**, 1571.
25 J. L. Baudour, Y. Delugeard and M. Sanquer, *Acta Crystallogr., Sect. B*, 1974, **30**, 691; Y. Delugeard, J. Desuche and J. L. Baudour, *Acta Crystallogr., Sect. B*, 1976, **32**, 702.
26 S. Janitz, D. D. C. Bradley, M. Grell, C. Giebeler, M. Inbasekaran and E. P. Woo, *Appl. Phys. Lett.*, 1998, **73**, 2453.
27 C. Botta, S. Destri, W. Porzio, A. Borghesi, A. Sassella, R. Tubino, G. Bongiovanni, M. A. Loi and A. Mura, *Phys. Rev. B*, 1999, **60**, 6039.
28 V. N. Bliznyuk, S. A. Carter, J. C. Scott, G. Klärner, R. D. Miller and D. C. Miller, *Macromolecules*, 1999, **32**, 361.
29 A. Hindeleh and R. Hosemann, *J. Phys. C*, 1988, **21**, 4155 and references therein.
30 R. N. Marks, J. J. M. Halls, D. D. C. Bradley, R. H. Friend and A. B. Holmes, *J. Phys. Condens. Matter*, 1994, **6**, 1379.
31 J. S. Kim, R. H. Friend and F. Cacialli, *Appl. Phys. Lett.*, 1999, **74**, 3084; X. Long, A. Malinowsky, D. D. C. Bradley, M. Inbasekaran and E. P. Woo, *Chem. Phys. Lett*, 1997, **272**, 6.
32 A. Altomare, M. Camalli, G. Cascarano, C. Giacovazzo, A. Guagliardi, M. C. Burla and G. Polidori, *J. Appl. Crystallogr.*, 1989, **22**, 389.